ARTICLE

Significant Enhancement in Built-in Potential and Charge Carrier Collection of Organic Solar Cells using 4-(5-hexylthiophene-2-yl)-2,6-bis(5-trifluoromethyl)thiophen-2-yl)pyridine as a Cathode Buffer Layer

Yue Zang[a], Kang-li Cao[b], Jiang Huang[a], Qing Zhang[b*], Jun-sheng Yu[a*]

a. State Key Laboratory of Electronic Thin Films and Integrated Devices, School of Optoelectronic Information, University of Electronic Science and Technology of China, Chengdu 610054, China
b. Department of Polymer Science, School of Chemistry and Chemical Technology, Shanghai Jiao Tong University, Shanghai 200240, China

(Dated: Received on May 8, 2014; Accepted on July 21, 2014)

An electron transporting material of TFTTP (4-(5-hexylthiophene-2-yl)-2,6-bis(5-trifluoromethyl)thiophen-2-yl)pyridine) was investigated as a cathode buffer layer to enhance the power efficiency of organic solar cells (OSCs) based on subphthalocyanine and C_{60}. The overall power conversion efficiency was increased by a factor of 1.31 by inserting the TFTTP interfacial layer between the active layer and metallic cathode. The inner mechanism responsible for the performance enhancement of OSCs was systematically studied with the simulation of dark diode behavior and optical field distribution inside the devices as well as the characterization of device photocurrent. The results showed that the TFTTP layer could significantly increase the built-in potential in the devices, leading to the enhanced dissociation of charge transfer excitons. In addition, by using TFTTP as the buffer layer, a better Ohmic contact at C_{60}/metal interface was formed, facilitating more efficient free charge carrier collection.

Key words: Organic solar cells, Cathode buffer layer, Built-in potential, Charge carrier collection, Optical spacer effect

I. INTRODUCTION

Organic solar cells (OSCs) have recently attracted broad research interests due to their easy fabrication, low lost, mechanical flexibility, and lightweight [1−3]. Significant progress in improving the power conversion efficiency has been made over the past few years by illuminating device mechanisms, synthesizing high performance materials, and developing new device architectures [4−6]. These efforts have led to very encouraging efficiency of 8%−9% [7−9]. Besides, to improve the device performance, it has been recognized that the introduction of a buffer layer to optimize the contact between active layer and electrode is an effective method [10, 11]. Currently, the most commonly used cathode buffer layers in small molecular OSCs are organic electron transporting materials with a wide energy gap, such as bathocuproine (BCP) [12], bathophenanthroline (BPhen) [13], tris(8-hydroxy-quinolinato) aluminum (Alq_3) [14], bipyridyl-substituted oxadiazole, and 1,3,5-tris(2-*N*-phenylbenzimidazolyl) benzene (TPBi) [11].

The cathode buffer layer has multiple functionalities. Firstly, such transparent layer can avoid absorbing light reflected from metal electrode and act as an optical spacer to maximize the optical field at the active donor/acceptor interface, where the free charge carriers generate [15]. Secondly, it also forms a passivating layer to protect the underlying acceptor material from being damaged during the evaporation of hot cathode metal atoms [16]. Thirdly, it serves as an exciton blocking layer to prevent excitons generated in the acceptor from quenching at the cathode contact [12]. Fourthly, the cathode buffer layer should have good electron transporting ability to provide efficient charge collection at cathode [17]. Moreover, it was recently demonstrated that the cathode buffer layer contributed to the improvement in the dissociation process of charge transfer excitons (CTE) due to the increased built-in potential [18]. However, so far the effect of cathode buffer layer on the enhancement of device performance is under debate. A systematic study of the relationship between cathode buffer layer and the OSC characteristics requires further in-depth investigation. And clarifying the effect of the buffer layer will be helpful to modify the organic/electrode interface and greatly increase the device performance.

In this work, an electron transporting material TFTTP (4-(5-hexylthiophene-2-yl)-2,6-bis(5-trifluoromethyl)thiophen-2-yl)pyridine) was investi-

*Authors to whom correspondence should be addressed. E-mail: qz14@sjtu.edu.cn, jsyu@uestc.edu.cn

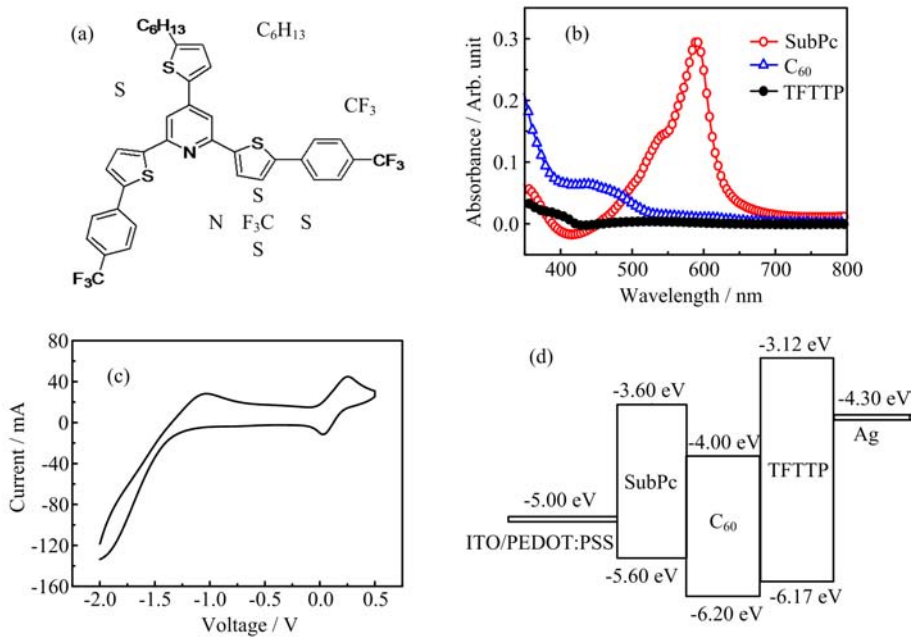

FIG. 1 (a) Chemical structure of TFTTP, (b) UV-Vis absorption spectra of SubPc, C_{60}, and TFTTP films, (c) cyclic-voltammetry data of TFTTP, and (d) schematic energy level diagram of OSCs.

gated as a cathode buffer layer in planar heterojunction organic solar cells. By inserting the TFTTP interfacial layer between active layer and metal cathode, the overall power conversion efficiency was increased by a factor of 1.31. In order to analyze the role of the TFTTP layer in OSCs, the optical field distribution and the photocurrent density characteristics of devices were studied in detail. Also, the dark diode behavior of the devices was simulated and discussed to further investigate the mechanism responsible for the efficiency enhancement by introducing TFTTP as the cathode buffer layer. All the results indicated that the introduction of TFTTP layer can significantly increase the built-in potential in the devices and facilitate more efficient free charge carrier collection at cathode, whereas the effect of TFTTP as an optical spacer was minimal.

II. EXPERIMENTS

The structure of organic solar cell is indium-tin oxide (ITO)/poly(3,4-ethylenedioxythiophene): poly(styrene-sulfonate) (PEDOT:PSS) (20 nm)/subphthalocyanine (13 nm)/C_{60} (35 nm)/(TFTTP) (x nm)/Ag (100 nm), x=0, 3, 5, 10, and 15. The devices were fabricated on the ITO coated glass substrates. The thickness of ITO film was ∼180 nm with a sheet resistance of 10 Ω/sq. The ITO substrates were cleaned consecutively in ultrasonic bath including detergent, acetone, ethanol, deionized water for 10 min each step, and finally dried by high purity nitrogen blow. Prior to loading into a vacuum chamber, the substrates were treated by O_2 plasma for 5 min. A thin layer of PEDOT:PSS film (Baytron P AI4083) was spin-coated onto the ITO glass with a rate of 5000 r/min for 40 s and then thermally annealed at 170 °C for 10 min in ambient. Organic materials were evaporated successively onto the ITO/PEDOT:PSS substrates by an organic multifunctional vacuum deposition apparatus at a rate of 1−2 Å/s at pressure of 3×10^{-4} Pa. Finally, Ag was evaporated as the cathode at a rate of ∼10 Å/s under pressure of 3×10^{-3} Pa without breaking the vacuum. The deposition rate and film thickness were *in situ* monitored using a QCM mounted to the substrate holder. The typical area of organic solar cells, defined by shadow mask, was 12 mm^2. The current density-voltage (J-V) curves in dark and under illumination were measured with a Keithley 4200 programmable voltage-current source. A light source integrated with a xenon lamp (CHF-XM35) with an illumination power of 100 mW/cm^2 was used as a solar simulator [5, 10, 11]. The UV-Vis absorption spectra were measured with a Shimazu UV-1700 system. All the measurements were performed in air at room temperature.

III. RESULTS AND DISCUSSION

The chemical structure of TFTTP is shown in Fig.1(a). TFTTP has been chosen as a cathode buffer layer in SubPc/C_{60} based device, since it has high optical transparency compared with the active materials of SubPc and C_{60}. Figure 1(b) shows the absorption spectra of organic films. It can be seen that TFTTP

DOI:10.1063/1674-0068/27/05/593-599

TABLE I Photovoltaic performance of the cells with various thicknesses of TFTTP layer determined from *J-V* characterization, where J_{max} is short-current density derived from simulated absorption spectra.

Thickness/nm	V_{OC}/V	J_{SC}/(mA/cm^2)	FF	η_p/%	J_{max}/(mA/cm^2)	R_SA/Ω·cm^2
0	0.66	2.84	0.29	0.54	7.55	128.28
3	0.77	3.14	0.37	0.89	7.65	22.26
5	0.82	3.67	0.35	1.05	7.69	22.09
10	0.80	4.10	0.38	1.25	7.67	12.40
15	0.77	3.46	0.33	0.88	7.51	20.06

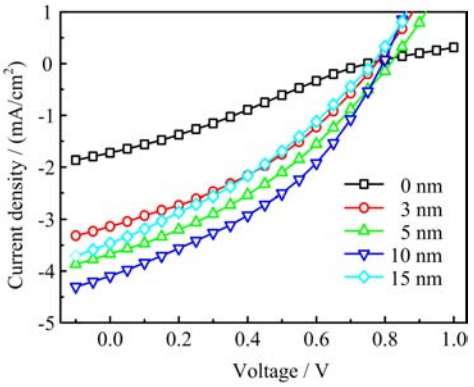

FIG. 2 *J-V* characteristics of OSCs with various TFTTP thicknesses under illumination with an intensity of 100 mW/cm^2.

is almost transparent in the full UV-visible range, and therefore does not significantly contribute to the absorption of SubPc/C_{60} device. The band gap energy of TFTTP was determined to be 3.05 eV corresponding to the on-set absorption energy. This large energy gap can efficiently block excitons from passing through the active layer. The lowest unoccupied molecular orbital (LUMO) level of TFTTP was determined to be around −3.12 eV by the cyclic-voltammetry data as shown in Fig.1(c). Therefore, the highest occupied molecular orbital level (HOMO) of TFTTP was −6.17 eV. Figure 1(d) shows the schematic energy level diagram of device used TFTTP as the cathode buffer layer.

J-V characteristics of OSCs with various TFTTP thicknesses under illumination with an intensity of 100 mW/cm^2 are shown in Fig.2. The detailed information on short circuit current (J_{SC}), open circuit voltage (V_{OC}), fill factor (FF), and power conversion efficiency (η_p), derived from the *J-V* curves are listed in Table I. It can be seen that V_{OC} increases from 0.66 V to 0.77 V when a 3 nm thick TFTTP inserted between C_{60} and Ag. This enhancement is attributed to the increase of built-in potential and the decrease of saturated dark current [19, 20]. Then V_{OC} is relatively constant at 0.80 V, independent of the thickness of TFTTP layer. The reason is that V_{OC} is predominately determined by the energy difference between the HOMO of donor material (D) and the LUMO of acceptor material (A) [21]. Moreover, J_{SC} and FF increase significantly initially and reach a maximum value in the device with 10 nm thick TFTTP. Once the TFTTP layer is thicker than 10 nm, J_{SC} and FF decrease. As a result, the device with a structure of ITO/PEDOT:PSS (20 nm)/SubPc (13 nm)/C_{60} (35 nm)/TFTTP (10 nm)/Ag (100 nm) shows the highest η_p of 1.25% with J_{SC}=4.10 mA/cm^2, V_{OC}=0.80 V, and FF=0.38. Furthermore, compared with the efficiency of the cell without a cathode buffer layer, the efficiencies of each cell with a TFTTP layer are dramatically enhanced. However, the overall performance is lower than those of other reports [22] with an almost identical architecture. We ascribed the loss to the comparatively high impurity density of organic materials and exposure to atmosphere during measurement, which would greatly reduce the charge carrier mobility [23].

For comparison, the photovoltaic characteristic of the cell with 10 nm BCP as the cathode buffer layer is also shown in Fig.3(a). The device exhibits a power conversion efficiency of 1.04% with J_{SC}=3.37 mA/cm^2, V_{OC}=0.88 V, and FF=0.35. It is worth to note that with the optimal thickness of 10 nm TFTTF layer, the efficiency of the cell is higher than that of BCP based cell due to the enhancement of J_{SC}. The relatively high η_p obtained for TFTTP based device may be attributed to the high electron mobility, which improves the charge transport and collection.

The electron mobility of TFTTP and BCP were measured from the field dependent space-charge-limited current (SCLC) model [24]. Figure 3(b) presents the *J-V* characteristic of electron only device with a structure of Ag (100 nm)/TFTTP (or BCP, 70 nm)/Ag (100 nm). The fitting result is also shown. TFTTP has a relatively high electron mobility of about 2.10×10^{-5} cm^2/V s, which is significantly higher than that of BCP (3.10×10^{-6} cm^2/V s). The lower electron mobility of BCP may lead to a relative higher series resistance (R_SA) of OSC devices [25]. The R_SA calculated from the *J-V* curves are 12.40 Ω·cm^2 and 22.52 Ω·cm^2 for TFTTP and BCP based devices, respectively. It has also been reported that higher carrier mobility of cathode buffer layer may enhance the OSC performance in terms of power conversion efficiency, due to the adequacy of the photogenerated electron being transported to the cathode [26]. Therefore, interfacial materials with high charge mobility should be optimized

DOI:10.1063/1674-0068/27/05/593-599

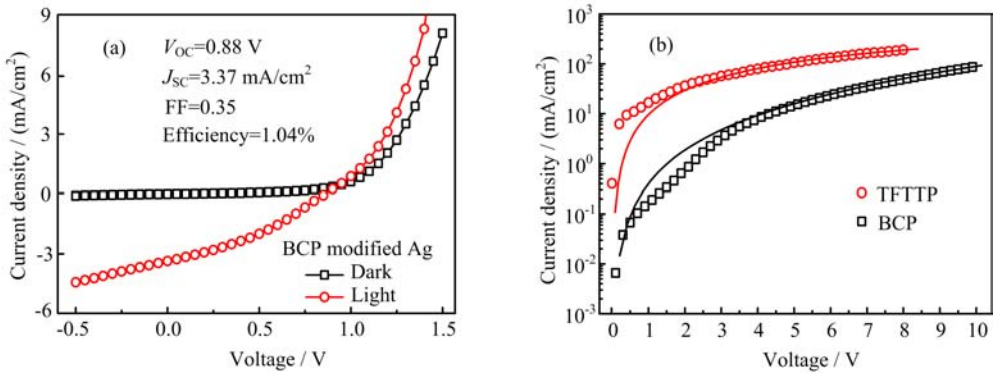

FIG. 3 (a) *J-V* characteristics of OSCs with 10 nm BCP as a cathode buffer layer in dark and under illumination, (b) *J-V* characteristics of electron-only device with a structure of Ag (100 nm)/TFTTP (or BCP, 70 nm)/Ag (100 nm). The symbols are experimental data for electron transport, while the solid lines are the fitting results according to the field-dependent SCLC theory.

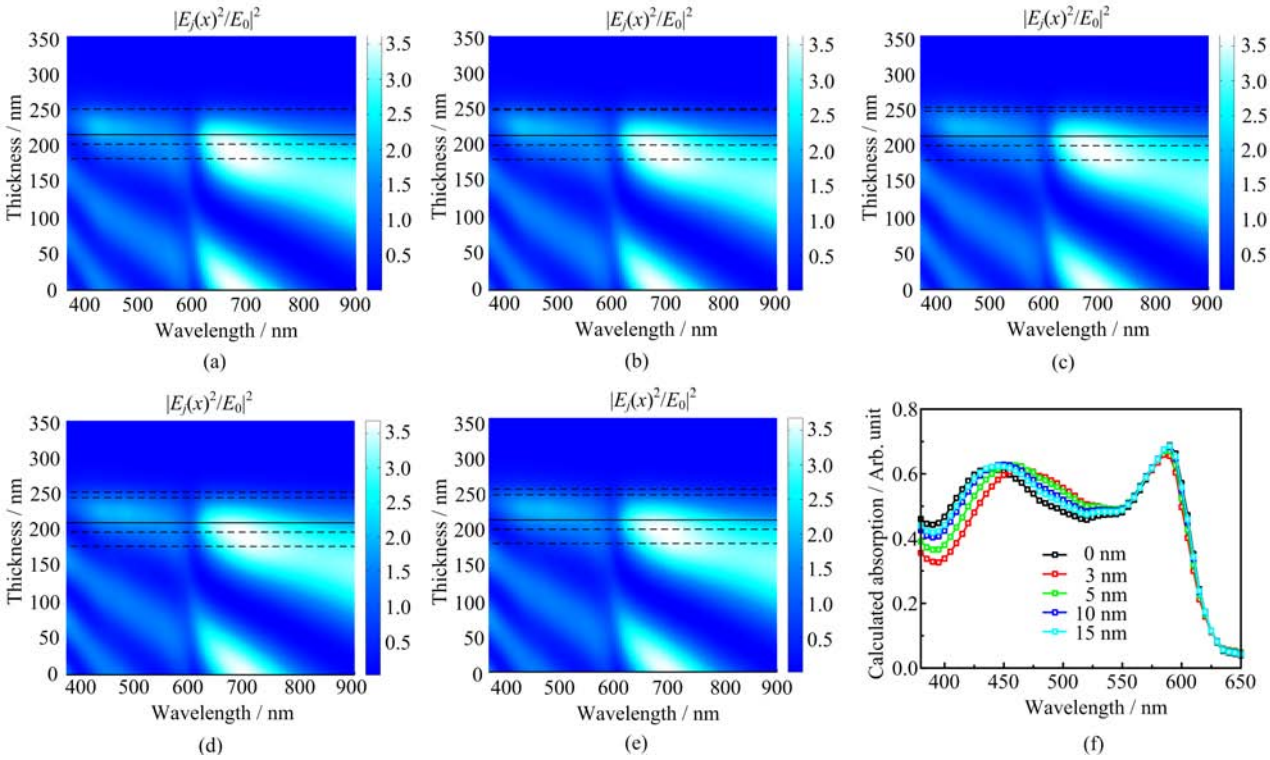

FIG. 4 Normalized electric field optical distribution in OSC devices with different TFTTP thickness of (a) 0 nm, (b) 3 nm, (c) 5 nm, (d) 10 nm, (e) 15 nm. (f) Calculated absorption fraction in the active layer of devices with various thicknesses of TFTTP.

for higher device performance.

To scrutinize the contribution of cathode buffer layer to the improvement of device performance under short circuit condition, the optical spacer effect of TFTTP was investigated using a one-dimensional transfer matrix method to simulate the optical field distribution within the device [17]. The normalized optical electric field $|E_j(x)|^2/|E_0(x)|^2$ distributions of the OSC devices are presented in Fig.4 (a)−(e). We can see that the intensity maximum trends to shift to the center of active layer when TFTTP thickness increases from 0 nm to 15 nm. This enhancement may partially lead to the increase of photocurrent.

To quantitatively estimate the effect of the TFTTP layer on light absorption, the fraction of incident light intensity absorbed by the active layer was simulated based on the transfer matrix formalism. The absorption spectra are shown in Fig.4(f). It can be seen that when TFTTP was inserted between C_{60} and Ag and used as the cathode buffer layer, the light absorbed by

DOI:10.1063/1674-0068/27/05/593-599

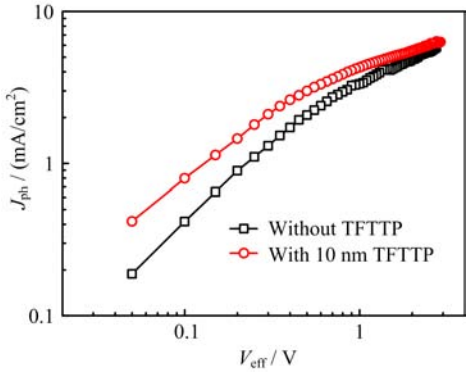

FIG. 5 Photocurrent density (J_{ph}) of OSCs without/with 10 nm TFTTP layers as a function of effective applied bias voltage (V_{eff}).

SubPc was increased, while the light absorbed by C_{60} was decreased. As a result, the introduction of TFTTP layer has a minimal effect on the total light absorption. Moreover, by integrating these spectra with the incident AM1.5G solar spectrum and assuming that internal quantum efficiency (IQE) is 100% [12], we can calculate the expected J_{max}, and these values are also given in Table I. We can see that the calculated data are significantly higher than the measured J_{SC}. This is induced by the energy loss origined from the inevitable recombination of excitons and charge carriers during transportation. It is also significant to note that the calculated J_{max} is only increased by 1.6% after modifying the cathode with 10 nm TFTTP. This indicates that the optical spacer effect of buffer layer is minimal, and the increase in J_{SC} is mainly due to the enhancement of internal quantum efficiency. However, when TFTTP thickness increases to 15 nm, the calculated J_{max} tends to decrease, resulting from the decreased electric field intensity in SubPc layer. This implies that a relatively thick TFTTP layer as an optical spacer may have a negative effect on the device performance.

In addition to the optical spacer effect, the R_SA can have a pronounced effect on J_{SC}, as shown in Table I. The R_SA was calculated from the nearly liner part (∼2.0 V) of the J-V curves. It can be found that the introduction of TFTTP significantly decreases the R_SA. Especially, at the optimal thickness of 10 nm TFTTP, R_SA decreased from 128.28 Ω·cm^2 to 12.40 Ω·cm^2. The reduction of R_SA is mainly due to the decrease of contact resistance. However, the further increase of TFTTP thickness to 15 nm results in an increase of R_SA to 20.06 Ω·cm^2. This is because that the thicker TFTTP layer introduces bulk resistance, which contributes to R_SA of the devices. The change of R_SA is in good agreement with the variation of J_{SC}.

It has been reported that the buffer layer can increase the photocurrent by preventing exciton from recombining at acceptor/cathode interface [17]. In order to quantify the influence of the buffer layer on exciton quenching, photocurrent density (J_{ph}) versus effective applied bias voltage ($V_{eff}=V_0-V$) is depicted in Fig.5. The photocurrent density is given by $J_{ph}=J_L-J_D$, where J_L and J_D are the current density under illumination and in the dark, respectively. The compensation voltage (V_0) is determined by the voltage at which $J_{ph}=0$. It can be seen that the introduction of TFTTP increases J_{ph}, which is 5.83 and 6.29 mA/cm^2 at high V_{eff} (∼3 V) without and with 10 nm TFTTP layers, respectively. Therefore, the large bandgap of TFTTP buffer layer can provide an energy barrier to exciton transport, and thus confine the excitons to the active layers, leading to an 8% increase of photocurrent. In addition to the exciton blocking effect, the increase of device performance is expected from the reduced non-radiative recombination of charge transfer excitons (CTEs), which has been identified as one of the main causes of energy loss in OSCs. From the normalized photocurrent density (J_{ph}/J_{sat}, here J_{sat} is the saturation photocurrent density), the CTE dissociation probability at $V=0$ is calculated, which increases from 48.54% to 65.02% after TFTTP was inserted.

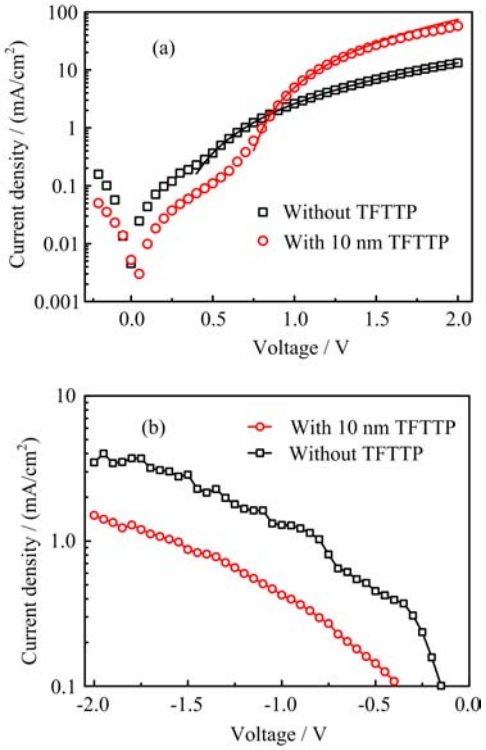

FIG. 6 (a) Dark J-V characteristics of OSCs without/with 10 nm TFTTP layers. The solid lines represent the fitting results using the Mott-Gurney law. (b) The saturation dark current density of the devices.

It has been reported that this enhancement may be due to the increase of internal electrical field (V_{bi}) [18]. Under short circuit condition ($V=0$), the CTEs generated at donor/acceptor interface can either decay to the ground state with a rate k_F or be separated into free charge carrier with a field-dependent rate of $k_D(E)$.

DOI:10.1063/1674-0068/27/05/593-599

Hence, the dissociation probability $P(E)$ is [27],

$$P(E) = \frac{k_{\rm D}(E)}{k_{\rm D}(E) + k_{\rm F}} \quad (1)$$

$$k_{\rm D}(E) = k_{\rm R}\frac{3}{4\pi a^3}\exp\left(-\frac{E_{\rm B}}{kT}\right)\cdot \left(1 + b + \frac{b^2}{3} + \frac{b^3}{18} + \frac{b^4}{180} + ...\right) \quad (2)$$

where $k_{\rm R}$ is the bimolecular rate constant of the bound e-h pair, a is the initial separation of bound e-h pair at the interface, $b{=}e^3E/8\pi\varepsilon\varepsilon_0k^2T^2$, $\varepsilon\varepsilon_0$ is the dielectric constant, and $E_{\rm B}$ is the CTE binding energy. An internal electric field can be obtained even at zero bias by using electrodes with different work functions. The built-in voltage in the device can be determined directly from the J-V measurements using the Mott-Gurney law [28],

$$J = \frac{9}{8}\varepsilon\varepsilon_0\mu\frac{(V - V_{\rm bi})^2}{d^3} \quad (3)$$

The dark J-V characteristics of OSCs without and with 10 nm TFTTP layers are shown in Fig.6. At higher voltage region where the flat band condition is reached, the measured current is dominated by space charge limited. It can be observed that in the case of bare Ag cathode, the device exhibits a $V_{\rm bi}$ of 0.2 V. After modifying the cathode with 10 nm TFTTP layer, the $V_{\rm bi}$ increases to ∼0.65 V. This enhancement of $V_{\rm bi}$ can prevent the geminate-pair from recombining at donor-acceptor interface, leading to the increase of photocurrent. However, it should be pointed out that a large external bias voltage is usually required to efficiently separate the electrons and holes, and thereby gives a CTE dissociation probability of 100%. It has been proven that in most polymer-fullerene systems, a reverse bias larger than 5−10 V (electric field of 25−50 V/μm for 200-nm-thick film) is required to dissociate the majority of CTEs at room temperature [29].

The enhancement of $V_{\rm bi}$ induced by TFTTP layer increases the $V_{\rm OC}$ of OSC as well. Figure 7 shows the energy band bending of OSCs under open circuit condition before and after modification with TFTTP buffer layers. It is known that the $V_{\rm OC}$ equals the energy difference between the electron and hole quasi-Fermi levels, which in turn are stated by the charge concentrations under steady-state illumination. As mentioned above, the field-dependent CTE dissociation process increases the charge density at the interface by reducing the recombination, and increases the quasi-Fermi level splitting between electron and hole, then contributes to the increase of $V_{\rm OC}$. In addition, the decrease of saturation dark current density also results in the improvement of $V_{\rm OC}$.

The TFTTP film was found to reduce the saturated dark current by a factor of 0.43, as shown Fig.6(b). The reduced saturated dark current should be ascribed to the formation of better Ohmic contact between C_{60} and Ag cathode. This is also constant with the decreased $R_{\rm S}$ after the introduction of TFTTP layer. This indicates that the recombination of charge carriers at C_{60}/Ag interface was reduced due to the better interface contact, leading to the improvement of carrier collection.

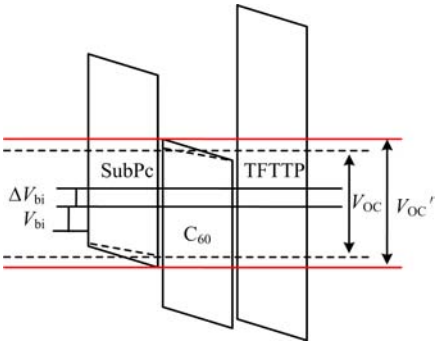

FIG. 7 Schematic energy level of the device under open circuit condition without/with TFTTP buffer layers.

IV. CONCLUSION

The effect of TFTTP as a cathode buffer layer on the performance of OSCs was studied. With the introduction of 10 nm TFTTP layer, the power conversion efficiency was increased by a factor of 1.31 primarily due to the increase in $J_{\rm SC}$ and FF. It was found that the enhancement of device performance was mainly contributed from the improvement of CTE dissociation efficiency due to the increased built-in potential. In addition, the use of TFTTP layer was beneficial for the formation of good Ohmic contact between C_{60} and Ag cathode, facilitating more efficient charger collection. Moreover, the simulation of optical field distribution inside devices showed that the optical spacer effect of TFTTP was minimal, whereas a relatively thick TFTTP layer decreased the light absorption efficiency. Therefore, the modification of organic/metal interface with a cathode buffer layer plays a critical role in the improvement of device performance. At an optimal film thickness, the TFTTP cathode buffer layer can both enhance the built-in potential to efficiently separate the charge transfer excitons (CTEs) and form a better contact to prevent the recombination of charge carriers at C_{60}/metal interface.

V. ACKNOWLEDGMENTS

This work was supported by the National Natural Science Foundation of China (No.61177032, No.21174084, and No.21274087), the Foundation for Innovative Research Groups of the Natural Science Foundation of China (No.61021061), and the Funda-

DOI:10.1063/1674-0068/27/05/593-599

mental Research Funds for the Central Universities (No.ZYGX2012YB025).

[1] J. Y. Kim, K. Lee, N. E. Coates, D. Moses, T. Q. Nguyen, M. Dante, and A. J. Heeger, Science **317**, 222 (2007).
[2] Y. Yang and F. Wudl, Adv. Mater. **21**, 1401 (2009).
[3] J. Huang, J. S. Yu, Z. Q. Guan, and Y. D. Jiang, Appl. Phys. Lett. **97**, 143301 (2010).
[4] J. Huang, Y. G. Qi, H. Y. Wang, and J. S. Yu. Appl. Phys. Lett. **102**, 183302 (2013).
[5] Y. Zheng, S. G. Li, X. G. Yu, D. Zheng, and J. S. Yu, RSC Adv. **4**, 16464 (2014).
[6] L. T. Dou, J. B. You, J. Yang, C. C. Chen, Y. J. He, S. Murase, T. Moriarty, K. Emery, G. Li, and Y. Yang, Nat. Photon. **6**, 180 (2012).
[7] Solarmer Energy Inc. breaks psychological barrier with 8.13% OPV efficiency, http://www.solarmer.com/news.php.
[8] Heliatek and IAPP achieve production-relevant efficiency record for organic photovoltaic cells, http://www.heliatek.com/index.php? Page=news.
[9] Mitsubishi Chemical To Commercialize Printable Solar Cells Next Year, http://techcrunch.com/2011/04/06/mitsubishi-chemical-to-commercialize-printable-solar-cells-next-year/.
[10] N. N. Wang, J. S. Yu, Y. Zang, J. Huang, and Y. D. Jiang, Sol. Energy Mater. Sol. Cells **94**, 263 (2010).
[11] J. S. Yu, N. N. Wang, Y. Zang, J. Huang, and Y. D. Jiang, Sol. Energy Mater. Sol. Cells **95**, 664 (2011).
[12] J. Huang, J. S. Yu, H. Lin, and Y. D. Jiang, J. Appl. Phys. **105**, 073105 (2009).
[13] M. Y. Chan, S. L. Lai, K. M. Lau, C. S. Lee, and S. T. Lee, Appl. Phys. Lett. **89**, 163515 (2006)
[14] Q. L. Song, F. Y. Li, H. Yang, H. R. Wu, X. Z. Wang, W. Zhou, J. M. Zhao, X. M. Ding, C. H. Huang, and X. Y. Hou, Chem. Phys. Lett. **416**, 42 (2005).
[15] J. Y. Kim, S. H. Kim, H. H. Lee, K. Lee, W. L. Ma, X. Gong, and A. J. Heeger, Adv. Mater. **18**, 572 (2006).
[16] H. Gommans, B. Verreet, B. P. Rand, R. Muller, J. Poortmans, P. Heremans, and J. Genoe, Adv. Funct. Mater. **18**, 3686 (2008).
[17] P. Peumans, A. Yakimov, and S. R. Forrest, J. Appl. Phys. **93**, 3693 (2003).
[18] Y. B. Yuan, T. J. Reece, P. Sharma, S. Poddar, S. Ducharme, A. Gruverman, Y. Yang, and J. S. Huang, Nat. Mater. **10**, 296 (2011).
[19] M. Vogel, S. Doka, C. Breyer, M. C. Lux-Steiner, and K. Fostiropoulosa, Appl. Phys. Lett. **89**, 163501 (2006).
[20] N. Li, B. E. Lassiter, R. R. Lunt, G. Wei, and S. R. Forrest, Appl. Phys. Lett. **94**, 023307 (2009).
[21] C. W. Chu, V. Shrotriya, G. Li, and Y. Yang, Appl. Phys. Lett. **88**, 153504 (2006).
[22] N. N. Wang, J. D. Zimmerman, X. R. Tong, X. Xiao, J. S. Yu, and S. R. Forrest, Appl. Phys. Lett. **101**, 133901 (2012).
[23] R. F. Salzman, J. Xue, B. P. Rand, A. Alexander, M. E. Thompson, and S. R. Forrest, Org. Electron. **6**, 242 (2005).
[24] B. P. Rand, J. G. Xue, S. Uchida, and S. R. Forrest, J. Appl. Phys. **98**, 124902 (2005).
[25] W. Y. Hung, T. H. Ke, Y. T. Lin, C. C. Wu, T. H. Hung, T. C. Chao, K. T. Wong, and C. I. Wu, Appl. Phys. Lett. **88**, 064102 (2006).
[26] S. W. Liu, C. C. Lee, C. F. Lin, J. C. Huang, C. T. Chen, and J. H. Lee, J. Mater. Chem. **20**, 7800 (2010).
[27] C. L. Braun, J. Chem. Phys. **80**, 4157 (1984).
[28] N. F. Mott and R. W. Gurney, *Electronic Processes in Ionic Crystals*, New York: Dover Publications, (1940).
[29] V. D. Mihailetchi, L. J. A. Koster, J. C. Hummelen, and P. W. M. Blom, Phys. Rev. Lett. **93**, 216601 (2004).

DOI:10.1063/1674-0068/27/05/593-599